Inelastic scattering of fast neutrons from ^{56}Fe

R. Beyer[1], *R. Schwengner*[1], *R. Hannaske*[1,2], *A. R. Junghans*[1], *R. Massarczyk*[1,2], *M. Anders*[1,2], *D. Bemmerer*[1], *A. Ferrari*[1], *T. Kögler*[1,2], *M. Röder*[1,2], *K. Schmidt*[1,2] *and A. Wagner*[1]
[1]Institute of Radiation Physics, Helmholtz-Zentrum Dresden-Rossendorf, 01328 Dresden, Germany
[2]Technische Universität Dresden, 01062 Dresden, Germany

Abstract
Inelastic scattering of fast neutrons from ^{56}Fe was studied at the photoneutron source nELBE. The neutron energies were determined on the basis of a time-of-flight measurement. Gamma-ray spectra were measured with a high-purity germanium detector. The total scattering cross sections deduced from the present experiment in an energy range from 0.8 to 9.6 MeV agree within 15% with earlier data and with predictions of the statistical-reaction code Talys.

1 Introduction

Cross sections of neutron-induced reactions attract growing interest in the context of future nuclear technologies. In particular, there is a need of data with high accuracy for neutron capture and fission induced by fast neutrons for isotopes of uranium, plutonium, and minor actinoids. In addition, cross sections of inelastic scattering of fast neutrons from structural materials, such as sodium, iron, and lead are of great interest [1].

The present work describes experiments studying the inelastic scattering of neutrons in the energy range from 0.8 to 9.6 MeV using the photoneutron source nELBE at the superconducting electron accelerator ELBE of the Helmholtz-Zentrum Dresden-Rossendorf (HZDR), Germany.

2 The photoneutron source nELBE

The photoneutron source nELBE consists of a circuit of liquid lead. The electron beam of about 3 mm in diameter passes a beryllium window and hits the liquid lead circulating in a molybdenum channel of 11.2 mm width. The intersection of the beam with the lead channel defines a volume of 0.6 cm^3. Liquid lead was chosen as the radiator material because the thermal load deposited by the electron beam (up to 25 kW) is too high to be dissipated from a solid target of such small size by gas cooling and heat radiation. Cooling with water is unfavorable because of neutron scattering and moderation. A detailed description of nELBE is given in Ref. [2].

The neutrons travelling at an angle of 95° relative to the incident electron beam enter the experimental area after passing a collimator in the concrete wall of 2.40 m thickness, followed by a 10 cm thick lead wall. The collimator consists of a combination of borated polyethylene and lead cylinders [2]. The experimental setup is schematically shown in Fig. 1. The neutron intensity was monitored with a calibrated ^{235}U fission chamber [3] delivered by the Physikalisch-Technische Bundesanstalt (PTB) Braunschweig. As no moderation was applied, the short accelerator beam pulses of about 5 ps provided the basis for a good time resolution for time-of-flight experiments at a flight path of 6.2 m. The neutron intensity at the target position was about 2×10^4 cm^{-2} s^{-1} using an electron bunch charge of 77 pC and a pulse repetition rate of (13 MHz)/64 = 203.125 kHz. Details of the neutron-beam profile, the determination of the neutron flux and the neutron spectrum are given in Ref. [4].

3 Experimental methods at the time-of-flight setup

The target consisted of a disk of natural iron with a diameter of 20 mm and a thickness of 8 mm with a mass of 19.787 g. This results in an areal density of $6.211 \cdot 10^{-2}$ ^{56}Fe atoms per barn. A high-purity

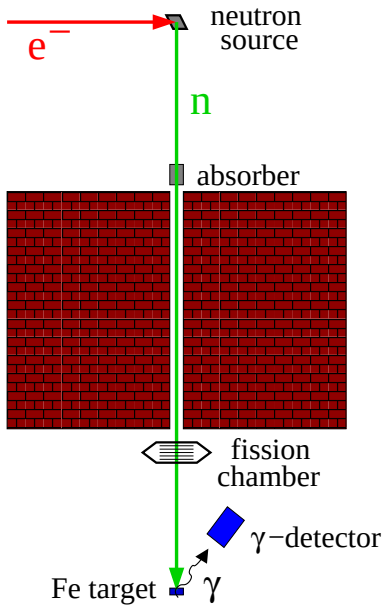

Fig. 1: (Color online.) Time-of-flight setup at the photoneutron source nELBE.

germanium (HPGe) detector with an efficiency of 100% relative to a NaI detector of 7.6 cm in diameter and in length was used to measure γ rays from states in ^{56}Fe. The detector was positioned at a distance of 20 cm from the target and at an angle of 125° relative to the beam direction. An energy and efficiency calibration of the detector was performed using ^{22}Na, ^{60}Co and ^{226}Ra standard calibration sources. The experiment was carried out with an electron beam energy of 30 MeV and an average current of 15 μA. The measurement was performed by cyclically placing the target in and out of the beam every hour to reduce long-term fluctuations of the beam current. The total live time of the measurement was 23 h for each case. The time of flight was measured as the time difference between the accelerator pulse and the signal of the HPGe detector. With this detector, a time resolution of 10 ns (FWHM) was achieved. The data acquisition recorded list-mode data containing signals of the fission chamber, the time-of-flight signal and the energy signal of the HPGe detector. Details of the system and of the dead-time correction are given in Ref. [4].

The calibration of the time-of-flight spectrum was performed as described in Ref. [4]. The time of flight was calculated according to

$$t_n = f \cdot (ch_n - ch_\gamma) + s/c, \tag{1}$$

where f = 0.9766 ns/channel, ch_n is the channel number in the time-of-flight spectrum, ch_γ is the channel number of the peak produced by bremsstrahlung scattered from the sample, s = 6175 mm is the flight path and c is the speed of light. Time-of-flight spectra for the measurements with and without target are shown in Fig. 2. The kinetic neutron energy E_n was derived as

$$E_n = m_n c^2 \left[\frac{1}{\sqrt{1 - s^2/(t_n c)^2}} - 1 \right], \tag{2}$$

where $m_n c^2$ is the neutron rest energy. The measured events containing time-of-flight and γ-ray energy were corrected for dead time and sorted into coincidence matrices for the measurements with and without target. The matrix containing events without target was subtracted from the one with target to reduce background events. Gamma-ray spectra were extracted by setting gates of 12 channels width, corresponding to 11.72 ns, on the time axis in the net matrix after background subtraction. An example

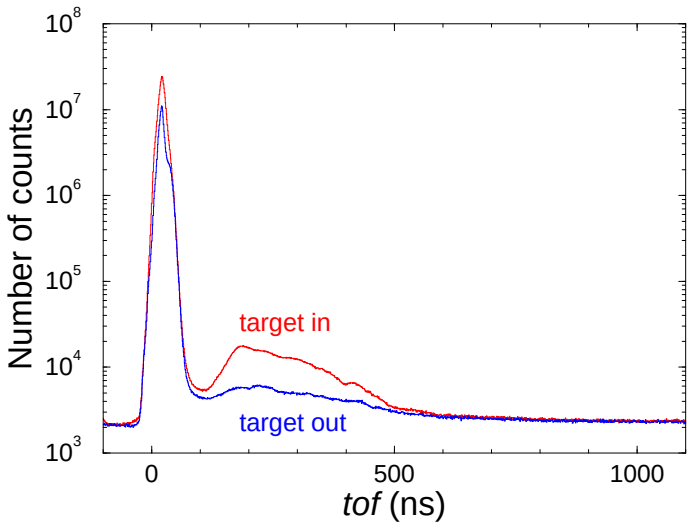

Fig. 2: Time-of-flight spectra with and without target containing events registered in the HPGe detector relative to the accelerator pulse.

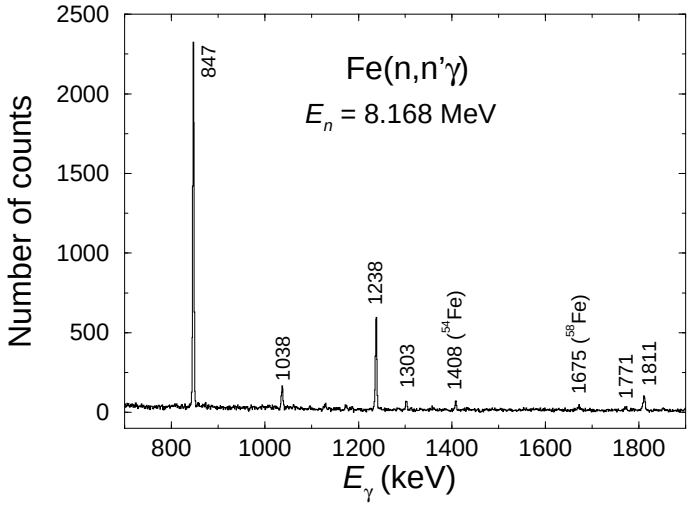

Fig. 3: Gamma-ray spectrum measured in the Fe$(n, n'\gamma)$ reaction for a neutron energy around E_n = 8.168 MeV. The time-of-flight gate width of 11.72 ns corresponds to a neutron-energy gate width of ΔE_n = 1.229 MeV. The labels denote energies of transitions in ^{56}Fe unless given otherwise.

of a resulting γ-ray spectrum is shown in Fig 3. The spectrum shows transitions between excited states in ^{56}Fe and, in addition the $2_1^+ \rightarrow 0_1^+$ transitions in ^{54}Fe and ^{58}Fe.

The neutron fluence (time-integrated flux) determined with the fission chamber for the present measuring time is shown in Fig. 4. The neutron flux was corrected for attenuation of the neutron beam in the target. The determination of the neutron flux using the fission chamber is described in detail in Ref. [4].

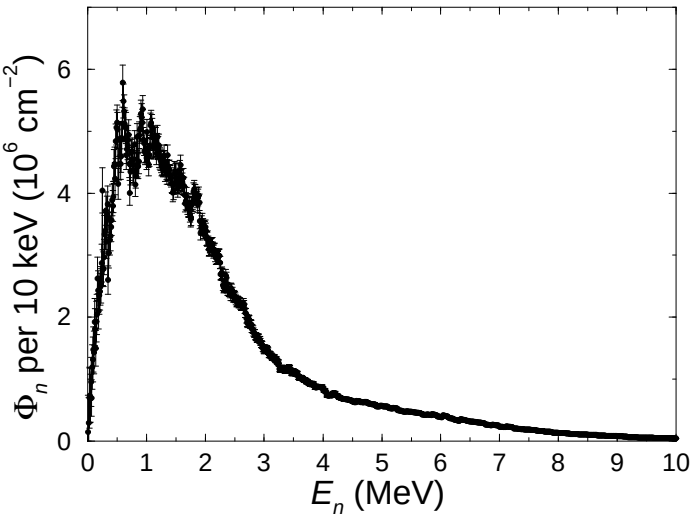

Fig. 4: Neutron fluence determined for the present experiment according to the procedure described in Ref. [4].

4 Experimental results

The reaction cross sections σ for excited states with energies E_i emitting γ rays of energy E_γ were calculated using the relation

$$\sigma(E_i, E_n) = \frac{N(E_\gamma, E_n)}{\varepsilon(E_\gamma)\Phi(E_n)N_{\rm at}}, \tag{3}$$

where $N(E_\gamma, E_n)$ is the number of dead-time corrected events in the peak at E_γ observed at a neutron energy E_n, $\varepsilon(E_\gamma)$ is the absolute efficiency of the HPGe detector at E_γ, $\Phi(E_n)$ is the neutron fluence at E_n, and $N_{\rm at}$ is the number of atoms in the target.

The cross sections obtained in this way were corrected for the attenuation of the emitted γ rays in the target material. The attenuation was simulated for γ rays emitted isotropically from the target. The start positions of the γ rays were distributed uniformly perpendicular to the beam direction and exponentially in beam direction because of the decreasing neutron intensity. For γ rays moving in the direction toward the detector the path length through the target $l_{\rm path}$ was calculated. The attenuation of the γ rays was described by an exponential distribution using the attenuation factors μ/ρ taken from Ref. [5] as mean values. From this distribution an attenuation length $l_{\rm att}$ was randomly sampled for each photon. If $l_{\rm att} < l_{\rm path}$, then the photon is absorbed in the target. The correction factors C applied to the cross sections are the ratios of started photons to absorbed photons. The mean value of the path lengths was 5.16 mm assuming an average total cross section of 4 b for calculation of the attenuation of the neutron intensity. A change of this value by $\pm$ 4 b resulted in a change of C by less than 1%.

For high-energy neutrons, there exists a certain probability that they can be inelastically scattered more than once inside the target. This multiple scattering increases the cross section of an excited state at a certain neutron energy, although the multiply scattered neutron has an energy different from the incident energy. The increase is expected to be considerable in particular for the lowest excited state, namely the first 2^+ state in ^{56}Fe. The probability P for multiple scattering with the detection of the 847 keV γ ray in a subsequent scattering step was simulated with the code GEANT4 [6]. The cross section of the 2^+ state was corrected with the factor $(1 - P)$.

At the angle of $\theta = 125^\circ$ between detector and neutron beam direction, the term $A_2P_2(\cos\theta)$ of the expression for the angular distribution approaches zero. Nevertheless, the term $A_4P_4(\cos\theta)$ may produce a deviation of the angular distribution from unity, for example for a $2 \rightarrow 0$ transition. Feeding

from higher lying states attenuates the angular distribution. This means, the term may be applied to the 847 keV transition at energies below the next higher state, i.e. below about 2.1 MeV. Angular distributions of the 847 keV γ rays emitted in the ^{56}Fe reaction were measured in Ref. [7]. The coefficients A_2 and A_4 deduced from these measurements are listed in Table 1.

Table 1: Angular distribution coefficients of the 847 keV γ ray at various neutron energies, taken from Ref. [7].

E_n (MeV)[a]	A_2^b	A_4^b	$W(125°)^c$
0.93	0.521(30)	–0.511(33)	1.193(13)
0.98	0.539(13)	–0.302(14)	1.113(5)
1.08	0.435(17)	–0.144(19)	1.053(7)
1.18	0.398(39)	–0.331(44)	1.125(17)
1.28	0.312(31)	+0.020(4)	0.990(2)
1.38	0.396(18)	+0.039(20)	0.982(8)
1.59	0.319(22)	–0.167(25)	1.062(10)
1.68	0.226(12)	–0.155(15)	1.058(6)
1.79	0.216(10)	–0.082(13)	1.030(5)
1.85	0.245(31)	–0.089(36)	1.033(14)
2.03	0.190(18)	–0.023(21)	1.008(8)

[a] Neutron energy.
[b] Coefficients of the angular distribution $W(\theta) = 1 + A_2 P_2(\cos\theta) + A_4 P_4(\cos\theta)$ taken from Ref. [7].
[c] Angular distribution $W(\theta = 125°)$ calculated using the given A_2 and A_4 values.

The largest A_4 value was found at the lowest neutron energy. This value amounts to 30% of the maximum value of $A_4^{\max} = -1.714$ predicted for a $2 \to 0$ transition [8]. This attenuation may be caused by the reaction mechanism. The further values generally decrease with increasing neutron energy. However, the values at E_n = 1.28 and 1.38 MeV do not follow the general behavior and have an unpredicted sign, which may indicate uncertainties of the values not covered by the given errors. Therefore, a correction of the total scattering cross section deduced from the 847 keV transition for the angular distribution has not been applied. This concerns the values for neutron energies below 2.1 MeV. At higher energies, feeding from higher-lying states occurs and the angular distribution is further attenuated. For the $4 \to 2$ and $6 \to 4$ transitions the $A_4^{\max}$ values are -0.367 and -0.242, respectively. Assuming also an attenuation of about 30%, the contribution of $A_4 P_4(\cos 125°)$ to the angular distribution at 125° is 4.0% and 2.5%, respectively. For the 4^+ state, also feeding has been taken into account, which reduces the value of 4% further. For the 6^+ state, the mentioned value of 2.5% has also not been applied to the values shown in the following. The contribution of $A_4 P_4(\cos 125°)$ to the $2 \to 2$ transitions feeding the 2^+ state at 847 keV is less than 0.5%, also if taking into account a mixing ratio of $\delta = 0.25$ as recommended for the 2113 and 2523 keV γ rays [9].

The total inelastic scattering cross section can be deduced from the intensity of the respective $2_1^+ \to 0_1^+$ transition that collects all intensity from higher-lying states, whereas the intensities of other ground-state transitions can be neglected [9]. The total scattering cross section deduced in this way for ^{56}Fe is shown in Fig. 5. The error bars include statistical uncertainties of the γ-ray intensities and the total uncertainty of the neutron flux. Possible systematic uncertainties of the neutron flux are discussed in Ref. [4]. The cross section shows resonance-like structures at 1.2, 1.6 and 2.4 MeV and a flattening above about 6 MeV.

Total inelastic neutron-scattering cross sections calculated with the code Talys [10] on the basis of the statistical reaction model are compared with the present experimental values in Fig. 5. It can be seen that the calculations describe magnitude and gross behavior of the experimental cross section. However, the resonance-like structures observed at about 1.2, 1.6 and 2.4 MeV are not included in the statistical model.

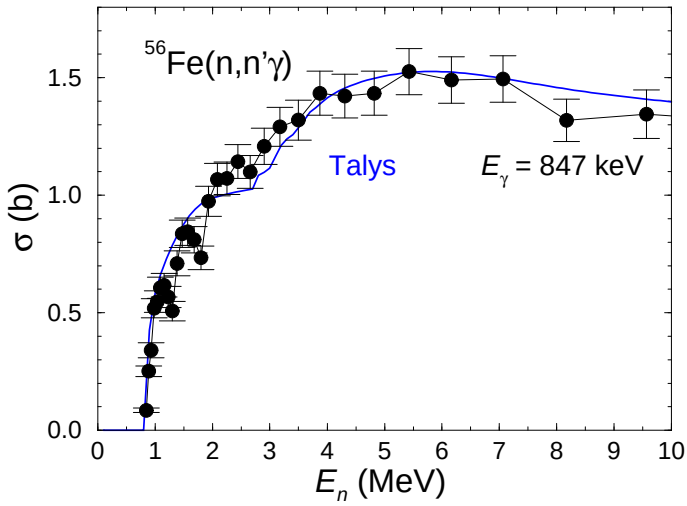

Fig. 5: (Color online) Total neutron-scattering cross section of ^{56}Fe deduced from the measured intensities of the 847 keV transition (black circles) and calculated with Talys (blue solid line).

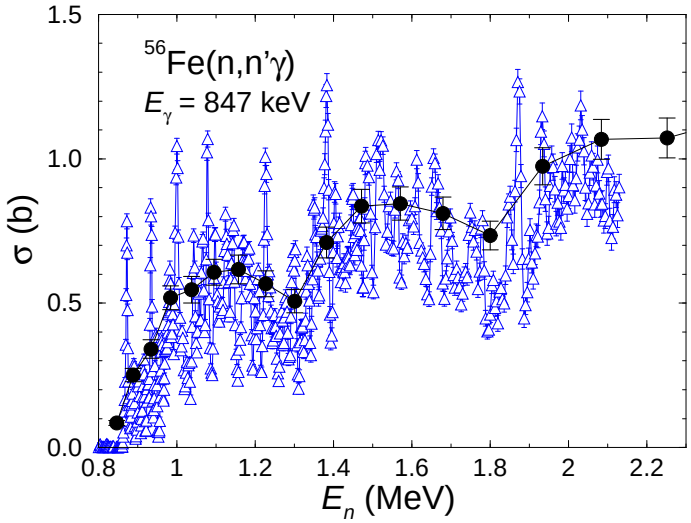

Fig. 6: (Color online) Total neutron-scattering cross section of ^{56}Fe deduced from the measured intensities of the 847 keV transition of the present work (black circles) and of Ref. [11] (blue triangles).

The total inelastic scattering cross section deduced in an earlier experiment [11] is compared with the present one in Fig. 6. The smaller steps in neutron energy resulting from a better time resolution at a longer flight path reveal fluctuations in the cross section not resolved in the present measurement. The present data tend to be greater than the data of Ref. [11]. For a better comparison of the absolute values of the data of Refs. [11] and the evaluated data of Ref. [12] with the present ones, the data of Refs. [11, 12] were rebinned according to the present conditions and are compared with the present data in Fig. 7. This comparison shows that the present data tend to exceed the data of Ref. [11] by up to about 15% and the data of Ref. [12] by up to about 20%.

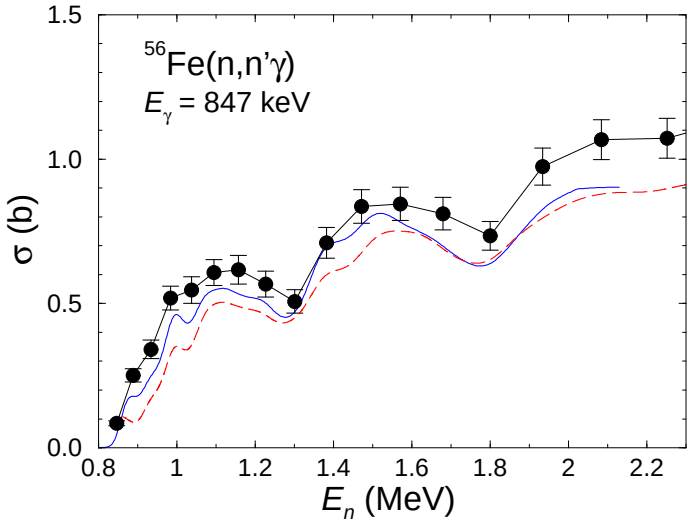

Fig. 7: (Color online) Total neutron-scattering cross section of ^{56}Fe deduced from the present data (black circles) in comparison with rebinned data of Ref. [11] (blue solid line) and of Ref. [12] (red dashed line).

5 Acknowledgments

Stimulating discussions with A. Plompen are gratefully acknowledged. We thank the staff of the ELBE accelerator for their cooperation during the experiment and A. Hartmann for the technical assistance. This work is supported by the German Federal Ministry for Education and Science within the TRAKULA project (02NUK13A) and by the European Commission within the projects EFNUDAT (FP6-036434) and ERINDA (FP7-269499).

References

[1] M. Salvatores, NEA/WPEC-26, OECD (2008); http://www.nea.fr/html/science/wpec/volume26/volume26.pdf.

[2] J. Klug, E. Altstadt, C. Beckert, R. Beyer, H. Freiesleben, V. Galindo, E. Grosse, A. R. Junghans, D. Legrady, B. Naumann, K. Noack, G. Rusev, K. D. Schilling, R. Schlenk, S. Schneider, A. Wagner, and F.-P. Weiss, Nucl. Instr. Meth. A 577 (2007) 641.

[3] R. Nolte, M. S. Allie, F. D. Brooks, A. Buffler, V. Dangendorf, J. P. Meulders, H.Schuhmacher, F. D. Smith, and M. Weierganz, Nucl. Sci. Eng. 156 (2007) 197.

[4] R. Beyer, E. Birgersson, Z. Elekes, A. Ferrari, E. Grosse, R. Hannaske, A. R. Junghans, T. Kögler, R. Massarczyk, A. Matic, R. Nolte, R. Schwengner, and A. Wagner, Nucl. Instr. Meth. A 723 (2013) 151.

[5] J. H. Hubbell and S. M. Seltzer, NIST Standard Reference Database 126 (2004).

[6] S. Agostinelli *et al.*, Nucl. Instr. Meth. A 506 (2003) 250.

[7] D. L. Smith, Argonne National Laboratory, report ANL/NDM-20, 1976.

[8] T. Yamazaki, Nucl. Data A **3** (1967) 1.

[9] H. Junde, H. Su, and Y. Dong, Nucl. Data Sheets 112 (2011) 1513.

[10] A. J. Koning, S. Hilaire, and M. C. Duijvestijn, AIP Conf. Proc. 769 (2005) 1154.

[11] F. G. Perey, W. E. Kinney, and R. L. Macklin, 3rd Conf. Neutron Cross-Sections + Technology, Knoxville 1971, vol. 1, p. 191.

[12] JEFF-3.1 evaluated data library; http://www.oecd-nea.org/dbforms/data/eva/evatapes/jeff_31/